

Improved Surface Temperature Identification Method for Remote Observations of Sample Return Capsules

Byrenn Birch^{*}, David Buttsworth[†] and Fabian Zander[‡]
University of Southern Queensland, Toowoomba, 4350, Australia

A new method for the identification of the peak temperature of the heat shield based on remote spectral irradiance measurements is proposed and tested through analysis of results from the Hayabusa sample return capsule. To identify the peak temperature of the heat shield, a parameterised empirical model for the surface temperature distribution on the geometry is developed, and is then used to simulate spectra for optimised fitting with a measured spectral radiance. This new peak temperature identification method is shown to be insensitive to the wavelengths resolved, the view of the geometry, and to measurement noise. The peak temperature of the Hayabusa capsule geometry at the representative condition considered (3330 K) was resolved to within 20 K for the three instruments investigated, while the effective temperature varied by around 600 K depending on which instrument was used. The error in the peak temperature model is also shown to be an order of magnitude less sensitive to measurement noise than the effective temperature approach. The new peak temperature method facilitates the direct comparison of results from instruments with different bandwidths and/or different view angles of the capsule, which was previously not possible.

I. Nomenclature

A_v	=	visible area
B	=	spectral radiance
c	=	speed of light
h	=	Planck constant
I	=	Intensity
I_{noise}	=	Intensity of noise
I_{syn}	=	Intensity signal generated from results of numerical studies
I_{Teff}	=	Intensity signal generated using an effective temperature

^{*}Lecturer, School of Engineering, AIAA Member; byrenn.birch@usq.edu.au.

[†]Professor, School of Engineering, AIAA Member.

[‡]Associate Professor, School of Engineering, AIAA Member.

$I_{T(s)}$	=	Intensity signal generated from the peak temperature model
k_B	=	Boltzmann constant
q	=	heat flux
q_0	=	stagnation point heat flux
q_r	=	radiative heat flux
R_b	=	cone base radius
r_c	=	radius at start of cone frustum
R_n	=	spherical nose radius
s	=	wetted length
s_c	=	wetted length to cone frustum
T	=	temperature of surface
T_0	=	temperature of surface at the stagnation point
T_e	=	temperature of the environment
T_{eff}	=	effective temperature of the geometry deduced through analysis
T_{max}	=	maximum temperature of the geometry specified a priori
T_{peak}	=	peak temperature of the geometry deduced through analysis
ϵ	=	emissivity
θ	=	angle around spherical nose
θ_c	=	nose half-angle
λ	=	wavelength
σ	=	Stefan-Boltzmann constant
τ	=	transmission
ϕ_c	=	local body angle

II. Introduction

FROM the earliest days of flight testing, visual observation and photographic records have played a critical role in the analysis of performance, verification of achievements, and documentation of failures. A photographic image showing the Wright brothers' first powered flight is preserved in a range of formats [1], demonstrating acquisition of ground-based optical data at the outset of powered, heavier-than-air flight. With the commencement of hypersonic flight testing, five 'chase aircraft' were commonly used during flights of the X-15 [2] and provided the X-15 pilots real-time visual confirmation of control surface attitudes and landing gear status and alerting test pilots to other potentially life-threatening problems such as fuel leaks. Photographic and video records from the Challenger and Columbia

Space Shuttle accidents contributed compelling evidence to subsequent forensic investigations [3, 4]. More recently, access-to-space missions by SpaceX and others companies have been thoroughly documented through surface-based and airborne videography. Such documentation enables broad public engagement and, when failures occur, assessment of the video records can also contribute to rapid system improvements.

Remote flight observation missions have been performed to assess turbulent heat transfer on the Space Shuttle tiles through spatially-resolved thermal imaging on multiple occasions [5–7]. Remote observation missions have also acquired spectral signatures during hypervelocity space capsule reentries including Genesis [8], Stardust [9], Hayabusa [10, 11], and Hayabusa2 [12–14]. Spectral signatures from hypervelocity geometries and the surrounding gas contain encoded information about high-temperature gas kinetics, thermal protection material response, and energy dissipation rates and processes [12]. Meteorites are also of interest, but embedding additional sensors in the object is not possible, so remote observation plays an important role in meteoritics and studies in the aerothermodynamics and demise processes that are needed to model the hazards associated with the debris field [15, 16]. Mitigating hazards and managing the environmental impact arising from the entry of space hardware is also important and further data are needed to improve the modelling of destructive reentry, so remote observation of such events is also an active area [9, 17, 18].

During scientific airborne observations, the high speed objects are generally so distant that is frequently impractical to use large enough magnification to directly provide spatial resolution; the objects appear as point sources on the imaging sensor [8–10, 12, 19]. When emissions from the shock layer are present, they appear on the imaging sensors as superimposed on emissions from the capsule surface. However, if the radiation signature is acquired with sufficient spectral detail, prior analyses have demonstrated that it is possible to distinguish gas-phase and capsule surface effects through the use of radiation models for the gas species and the capsule surface. By fitting multi-parameter zero-dimensional models to the experimental data, prior work has identified effective temperatures for the gas species and the capsule surface [20–22].

While effective temperatures can be deduced by fitting the spectral data acquired from capsules with zero-dimensional radiation models, alternative approaches have also been demonstrated using multi-dimensional computational simulation methods including radiation models with the viewable emissions summed over the computational domain for direct comparison to the experimental data. Effective temperatures can then be determined using virtual spectrometers or, since the distance, atmosphere and geometry are defined, a Planck curve can be fitted to the radiance at one or more wavelengths to determine the apparent temperature of the capsule. Using a multi-dimensional computational approach further enables the comparison of the high-order model with the measured data to investigate material response and thermochemistry in the shock-heated gas surrounding the capsule, provided that the real trajectory and view angles of the capsule can be accurately determined, and the heat shield material properties can be reasonably estimated [19, 23].

The remote spectral measurement of hypervelocity events is important to the understanding of such events and the

design of tools to better model hypervelocity flight and associated phenomena. To date, no spatially resolved data from remote spectral observations of super-orbital reentry events has been acquired because the necessary magnification has not been practical. High-order numerical methods have been used to generate spectral irradiance results from spatially resolved surface temperature and radiating gas fields, however these simulations currently produce results that differ from the experimental data markedly and are reliant on knowledge of the often proprietary heat shield material properties and object trajectory [19].

Sample return capsules are of sphere-cone (or similar) geometry, and this shape is also representative of the nose geometry of sustained hypersonic flight vehicles. The largest amount of publicly available experimental data and numerical results in the form of spectral signatures exists for the Hayabusa sample return capsule reentry [10, 23] and therefore forms the example case for this work. In this present work, a method for resolving surface temperature distributions on hypersonic sphere-cone geometries from remote spectral measurements is developed. This method overcomes the wavelength dependence of the effective temperature method and does not require detailed knowledge of the heat shield material properties.

III. Remote Spectral Imaging of Hypervelocity Events

The typically large distances required for the remote scientific observation of high speed objects, combined with the limited practical magnifications of the instruments used, results in the object of interest appearing as a point source on the imaging sensor. Therefore the raw image data lacks spatial resolution— for a measured spectral irradiance of an object travelling at hypersonic speeds, the gas radiation from the shock layer is superimposed on emissions from the capsule surface. The significance of the near-wake contributions to the spectral irradiance from the capsule are generally considered negligible when the angle between the sight vector and velocity vector of the capsule less is than the half-angle of the body [19, 20, 23]. The irradiance is attenuated by an intervening atmosphere between the capsule and the measurement location. When the capsule trajectory is defined, these atmospheric effects can be modelled and therefore compensated for in later data analysis.

The spectral emission of the hypervelocity body and the high-temperature gas surrounding it contains information about high-temperature gas kinetics, the response and performance of thermal protection systems, and energy dissipation rates and processes. Typical scientific objectives for remote observations of reentry events include: (1) the identification of thermal protection system properties via an effective temperature measurement; (2) radiance measurements of atomic and molecular line emission from the shock-heated air in the stagnation region; (3) assessment of rates of molecular recombination and species relaxation in the wake region; and (4) the detection and characterisation of ablation species. To achieve these objectives, a diverse range of spectral instruments can be deployed from ground-based and airborne observation platforms. The diversity of spectral instrumentation deployed for the airborne observation of the Hayabusa and Hayabusa2 reentries is illustrated using Figure 1 which shows the bandpass and spectral resolution of a selection of

instruments.

It must be noted that the bandpasses shown in Figure 1 are used to show the extent of the wavelengths for which useful data may be collected, however the actual bandpass width for any one frame may be practically limited by the sensor size and position of the capsule in the spectrometer field of view. Much of this instrumentation diversity can be attributed to the need to resolve atomic and molecular line emissions and characterise ablation species. Where line emissions and narrowband absorptions are present, these wavelengths can be masked from curve fitting routines to determine the effective capsule temperature [14]. Regardless of the instrument bandpass and spatial resolution, every instrument will record information that enables an effective temperature of the capsule to be determined if the instrument is well calibrated, inclusive of the effects of aircraft windows, and a reliable model for atmospheric absorption can be defined.

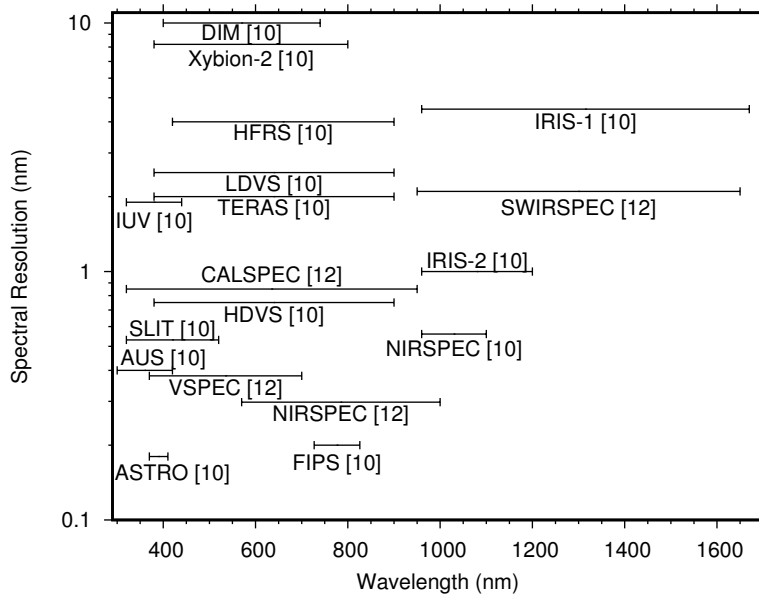


Fig. 1 Spectrometer dispersion and resolution for selected instruments used in the remote observation of the Hayabusa and Hayabusa2 capsule reentries.

The effective temperature of a reentry capsule is a somewhat limited metric— it is a function of the surface temperature distribution on the capsule, the geometry of the capsule, and of the angles at which the geometry has been imaged. If the instrument does not have an absolute calibration, or there are uncertainties therein, then the effective temperature is also a function of the wavelengths that have been resolved. The limitations of the effective temperature approach are demonstrated in Figure 2 using published results from ground and airborne observations of the Hayabusa reentry. Note that all data presented in Figure 2 were published with no, or incomplete, corrections for atmospheric extinction. Analysis of results from the ground-based CID instrument from 20 s onwards resulted in significant deviations from to the airborne results and other ground-based instrument shown (S2000). The effective

temperature identified from the S2000 instrument results agreed comparatively well with the results from the airborne instruments. The magnitude of the effective capsule temperature varies by several hundreds of degrees at all times, even when the outlying temperatures are neglected. Around peak heating, which occurred between 20 s and 25 s on the illustrated time scale, the variability of effective temperature of the capsule was around ± 250 K when the CID data is excluded. The time rate-of-change of effective temperature is in good agreement for the AUS and CCO instruments, but this time rate-of-change agreement does not extend to the JASMIN-1 instrument [24]. Some of the discrepancy in the apparent temperature results could be attributed to the quality of the experimental data, especially for the CID dataset. However, for the other results shown in Figure 2 it is likely that the different view angles and the resolved wavelengths have contributed to the variation of effective temperature identified from each instrument, a dependency which is demonstrated in Section VII.A.

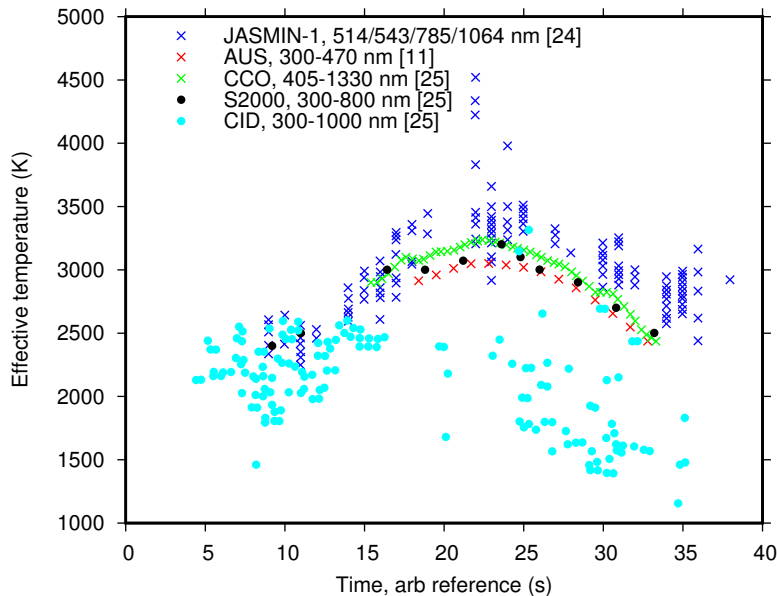


Fig. 2 Effective temperature (atmospheric extinction effects not considered) of the Hayabusa capsule during reentry as measured using instruments of varying bandpasses from airborne (shown with \times symbols) and ground-based platforms (shown with \bullet symbols).

The dominant uses for effective temperature measurements are the qualitative comparison of data obtained from different instruments and for comparison with simulated spectral radiance and spectral irradiance for model validation. To produce high fidelity simulated spectral intensity signals which contain the radiation from the capsule surface, knowledge of the surface temperature distribution on the heat shield surface is critical. However, many heat shield materials are proprietary so modellers must assume materials and material properties [19]. If the state of the boundary layer on the heat shield can be assumed, the self-similar normalised surface distribution on bodies in the hypersonic regime can be leveraged. Once the stagnation point temperature is determined, the temperature distribution over the heat shield surface is defined [19]. The method developed in this paper leverages the same self-similar temperature

distribution assumption as in [19] to identify surface temperature distributions on heat shield surfaces.

By identifying the temperature of the heat shield at the stagnation point remote spectral measurements can be compared with onboard data, provided that the onboard instrumentation suitably located for this comparison or suitable thermal models can be developed. In the case of Hayabusa2, nine thermocouples were present but only one was located in the heat shield [24].

IV. Surface Temperature of Sphere-Cone Geometries

A. Arrangement and Assumptions

The objective is to develop a model for the thermal emission signature of a generic object during hypersonic flight, and the geometry of the flight object being considered is illustrated in Figure 3. The end requirement of the procedure is a parameterised description of the surface temperature on a known geometry. This n-dimensional description can then be used as the basis function to identify the surface temperature distribution on the geometry from a measured radiance signal via a fitting optimisation routine. In the present model development work, we use empirical correlations to establish a parameterised surface temperature distribution function. Higher-order models such as the results from CFD could be used to develop this function, however as an independent source of higher-fidelity synthetic data for assessment could not be identified, the empirical form was used.

Development proceeds by introducing a model for the heat flux around the surface, from which local surface temperature and local spectral radiance can be estimated. The model thermal signature for the object is then obtained through integration across the viewable surface. The heat flux and other distributions around the sphere-cone are assumed axisymmetric, thus the assumed capsule angle of attack is 0° . A specific example is then considered: the Hayabusa capsule (defined in Table 1) is representative of blunt Earth-entry bodies and has been selected for the analysis in the present work due to the extent of publicly available experimental data and results from high-order simulations.

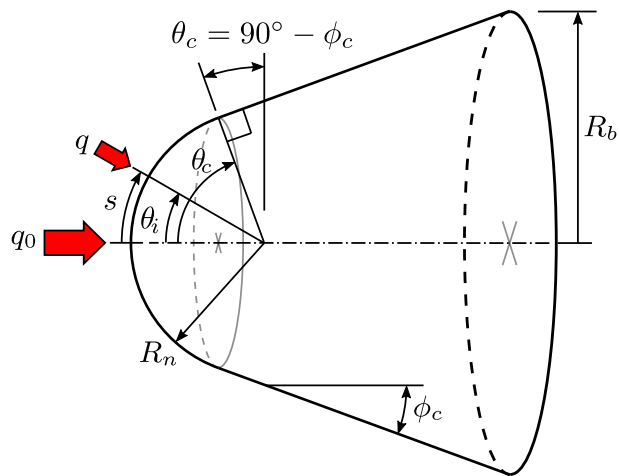


Fig. 3 Illustration of the generic sphere-cone arrangement.

Table 1 Geometry of the specific sphere-cone geometry presented herein.

Parameter	Hayabusa
Nose radius, R_n	200 mm
Base radius, R_b	200 mm
Cone half angle, ϕ_c	45°
Nose half angle, θ_c	90° - ϕ_c
Radius of cone frustum, r_c	$R_n \cdot \sin(\theta_c)$
Angle from nose, θ_i	$0^\circ \leq \theta_i \leq \theta_c$
Wetted distance from nose, s	$0 \leq s \leq s_c + \frac{R_b - R_n \cdot \cos \phi_c}{\sin \phi_c}$
Wetted length to cone frustum, s_c	$R_n \cdot \theta_c$

B. Parameterised Model Development

The local surface temperature of a geometry can be related to the heat flux around the geometry as a grey body such that that radiative emission is given by

$$q_r = \epsilon \sigma (T^4 - T_e^4)$$

where ϵ is the surface emissivity, σ is the Stefan-Boltzmann constant, and T is the local surface temperature and T_e is the environment temperature. For simplicity we treat the emissivity as a constant, and we expect that $T \gg T_e$. Invoking the equilibrium assumption in which the heat flux from the flow to the surface q is equal to the radiative heat loss from the surface, $q_r = q$, we have an expression for the relative variation of surface temperature

$$\frac{T}{T_0} \approx \left(\frac{q}{q_0} \right)^{\frac{1}{4}}. \quad (1)$$

where subscript 0 denotes stagnation point properties. There are numerous empirical forms to describe the heat flux around the spherical nose q relative to the stagnation point value q_0 . In this work we take an empirical correlation of the form presented in [26]

$$\frac{q}{q_0} = 1 + A\theta^2 + B\theta^4 \quad (2)$$

where A and B are constants that depend on the flight Mach number, and for compressible flow conditions, $A = -0.73$, $B = 0.16$ are reasonable approximations over the range $0 \leq \theta \leq 86.54^\circ$ based on data produced in a shock tube from Mach 7.6 to Mach 13.5 [27].

Along the conical frustum for wetted length $s \geq R_n \theta_c$, the heat flux is expected to decrease with increasing s unless

laminar-to-turbulent transition is a significant feature. For $s \geq R_n \theta_c$, and provided $\theta_c \leq 86.54^\circ$, we use the model

$$\frac{q}{q_0} = \left(1 + A\theta_c^2 + B\theta_c^4\right) \left(\frac{R_n \theta_c}{s}\right)^N \quad (3)$$

In the case of a laminar boundary layer, we expect that $N = 0.5$.

The equilibrium approximation will not correctly relate the heat flux and temperature distributions during rapid changes of vehicle attitude or speed; nor will it be applicable when surface ablation effects are non-negligible. However, the value of the approximation to the present work lies in the capacity to characterise the relative temperature variation.

The accuracy of Equation (1) is investigated using the spatially resolved heat flux and surface temperature results for the high-order simulation of the Hayabusa sample return capsule at 10.4 km s^{-1} (13:52:20 UTC) [28]. The maximum relative error resulting from Equation (1) on the spherical section of the Hayabusa forebody is $\Delta = 0.022$, and $\Delta = 0.032$ at the rear of the conical section, based on the simulations in [28].

Proceeding on the basis that Equation (1) is a useful approximation at all conditions of interest, Equation (1) can be combined with Equations (2) and (3) to show that

$$\frac{T(s)}{T_0} = \left[\left(1 + A \cdot \theta_c^2 + B \cdot \theta_c^4\right) \right]^{\frac{1}{4}}, \quad \text{for } \{0 \leq s \leq R_n \cdot \theta_c\} \quad (4)$$

$$\frac{T(s)}{T_0} = \left[\left(1 + A \cdot \theta_c^2 + B \cdot \theta_c^4\right) \left(\frac{R_n \cdot \theta_c}{s}\right)^N \right]^{\frac{1}{4}}, \quad \text{for } \left\{R_n \cdot \theta_c \leq s \leq s_c + \frac{R_b - R_n \cdot \cos \phi_c}{\sin \phi_c}\right\} \quad (5)$$

which forms the basis of the surface temperature curve fitting process presented in Section VI.

The suitability of the empirical model for normalised surface temperature distribution across a broader range of conditions is demonstrated using Figure 4 through a comparison to surface temperature distributions on the forebody of the Hayabusa sample return capsule as simulated in [23]. Strong agreement is found on the spherical nose of the capsule with a typical relative error of $\Delta = 0.0128$, with agreement found on the conical frustum to within $\Delta = 0.0344$. This agreement demonstrates that the surface temperature distribution on a sphere cone can be reasonably defined by its peak value, provided that the parameters A, B and N from Equations (4) and (5) are suitably defined. For all of the present work, $A = -0.73$, $B = 0.16$, and $N = 0.5$. Agreement with numerically-determined surface temperature distributions may be improved through parameter tuning or further empirical model development in future studies– the focus of the present work is method development and demonstration using published results from a high-order model. Such empirical models could include effects such as turbulent heating, if relevant to the geometry of interest.

The empirical model developed herein makes no attempt to model the hot shoulder of the capsule, which begins at $s \approx 210 \text{ mm}$ in Figure 4. The hot shoulder is not prominent in the work of [23] which justifies neglecting the hot shoulder in empirical model development. Through simulation of the Hayabusa2 emission spectral signature, the hot

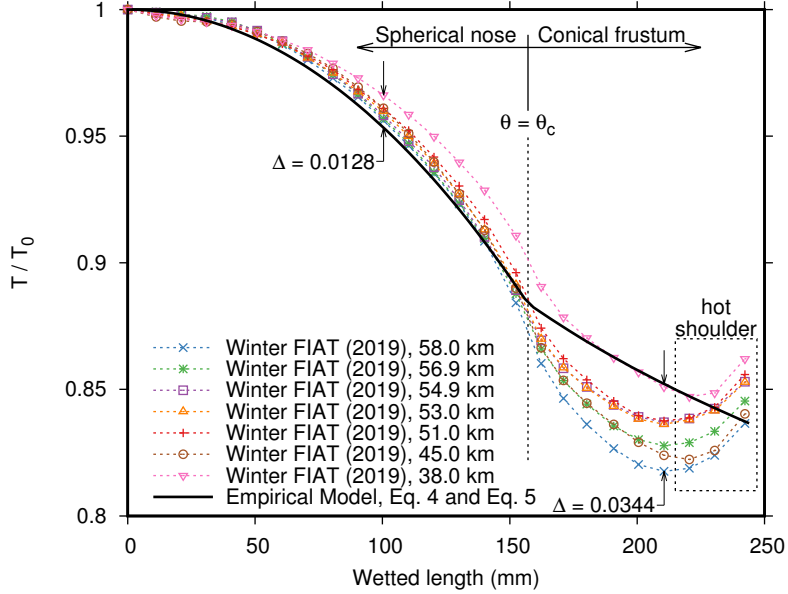


Fig. 4 Comparison of the normalised surface temperature distribution on the Hayabusa heat shield as calculated by [23] including material response and the empirical model presented in Section IV.B.

shoulder was found to increase the amplitude of irradiance with view angles (see Figure 5) from 0° to 5° as a greater proportion of this annular region comes into view, followed by a subsequent decrease after 5° [19]. However, the effect on neither the shape of the radiance curve nor the effective temperature was described. Additionally, the empirical model developed and presented herein makes no attempt to model the aft section (past maximum diameter) of a capsule geometry as the radiance is likely to be relatively small [19].

The wake will be of low significance to the signal for small view angles, but will increase in significance with increasing view angle as the visible volume of the wake increases. In the work of [23], the wake was found to not significantly contribute to the radiance and was therefore largely excluded from the radiation analysis (view angles from 17° to 56°) such that computational resources could be allocated to the shock layer volume. Unless the wake is significantly populated with ablated particles, the wake radiance is from low density and comparatively low temperature gas emissions which will appear in discrete bands and, like the shock layer, masked from the analysis of experimental data. Therefore the contribution of the wake to the radiance signal is also neglected in the present work.

V. Synthetic Spectral Intensity for Hypervelocity Vehicles

To investigate the performance of a method for the analysis of measured spectral irradiance, well defined test cases are required. Because of the limited real data available and the uncertainties associated with this data, synthetic spectral radiance and spectral irradiance are required. These synthetic signals allow the idealisation of spectral radiance and the selectable inclusion or exclusion of complexities such as: (1) atmospheric effects between the source and observer; (2) oblique viewing angles; (3) noise on the measured signals; (4) emissivity variations; and (5) shock layer and near-body

wake radiation. The effects of (1), (2), and (3) are treated, but (4) and (5) are considered beyond the scope of the present work.

The inclusion of wavelength and/or spatially varying emissivity (i.e material changes) could be readily considered with a priori knowledge of these properties. The contributions from the shock layer are known to be line emissions from the shock-heated gases, which can be readily identified and masked from studies of the surface temperature and therefore can be excluded from the spectra generation process in this context. The near-body-wake contributions are generally considered negligible when the angle between the sight vector and velocity vector of the capsule is less than the half-angle of the body [19, 20, 23], so minimal errors should be present in the synthetic spectra for view angles less than 23° for the Hayabusa sample return capsule.

The spectral radiance (B) of a black body at temperature T is given by

$$B(\lambda, T) = \frac{2hc^2}{\lambda^5} \frac{1}{\exp\left(\frac{hc}{\lambda k_B T}\right) - 1} \quad (6)$$

where λ is wavelength, h is the Planck constant, c is the speed of light and k_B is the Boltzmann constant. For bodies with a temperature that varies across the surface $T(s)$ but with emissivity that is dependent only on wavelength $\epsilon(\lambda)$ and a Lambertian surface, the spectral intensity of the body can be written

$$I(\lambda, T(s)) = \epsilon(\lambda) \frac{2hc^2}{\lambda^5} \int \frac{1}{\exp\left(\frac{hc}{\lambda k_B T(s)} - 1\right)} dA_v \quad (7)$$

where A_v is the surface area that is visible when projected onto the imaging plane for a given view orientation.

The contribution of the surface temperature aft of the maximum body radius of a capsule geometry is likely to be extremely small [19] and is therefore neglected herein, with the geometry therefore simplified to be only the geometry forward of the maximum body radius. Atmospheric effects can be included by simple multiplication of the transmission model with Equation (7).

By mapping the empirical surface temperature distribution to the simplified body representation, the view plane can be arbitrarily defined about the geometry to produce spectral signatures of the capsule surface radiation for any view angle. This imaging plane projection process follows the method of [19, 23] but excludes the radiating gases surrounding the capsule. In the work of [19, 23], the flowfield and material response is coupled to determine the surface temperature of the model. This approach is effective in the simulation of spectra, however, is computationally intensive which precludes this approach being applied to the direct analysis of experimental data. Substitution of the coupled CFD for a parameterised surface temperature model allows the analysis of experimentally acquired spectra while remaining computationally inexpensive. In this work the parameterised non-dimensional surface temperature distribution is described by the wetted length, s . The wetted length for the surface elements of a sphere-cone geometry can be readily

calculated, however this is not the case for all geometries of interest. Therefore, the 3-dimensional sphere-cone geometry considered in this work was imported as a standard triangle language file (*.stl) in preparation for the analysis of more complex geometries where s and the surface normal angles require significant analysis of the geometry. It is important to note that the *.stl file acts simply as a carriage for the geometry to the analysis script and therefore can be simply replaced by another convenient means for importing the geometry for surface temperature mapping if required. Although only sphere cones are being treated in the present work, the method can theoretically be applied to any geometry for which an empirical normalised surface temperature model can be developed. Geometries can include complex features which obscure the view of the dominant radiating surface such as on a hypersonic flight test vehicle.

VI. Methodology

The development and testing of the peak temperature identification method proceeds by producing synthetic spectral radiance signals using the method described in Section V for the Hayabusa sample return capsule. The synthetic spectral signatures were analysed using three virtual spectrometers that imitate the AUS [11], Hyper-IR [14] and SWIRSPEC [12] instruments which have been used to image the Hayabusa and Hayabusa2 reentries (see Figure 1). The full width of the sensor for each virtual instrument was assumed to capture a useful spectral intensity signal, representing the best possible case for a reentry observation. Since the quoted spectral bandwidth of the Hyper-IR instrument exceeds what can be resolved on the physical sensor for a single frame, the virtual Hyper-IR instrument was reduced to 600 nm to 968 nm with the 0.187 nm spectral resolution preserved. The entire resolvable spectral signature can be imaged in one frame for the AUS instrument so the virtual instrument matches the physical AUS instrument. The sensor matrix for the SWIRSPEC instrument was not identified so, for the purposes of a comparative analysis, the full reported spectral width for the SWIRSPEC instrument was used.

The limitations of effective temperature was established in Section III in the context of the remote observation of the Hayabusa sample return capsule. The primary task is to apply the peak temperature method to the analysis of synthetic spectral signatures (I_{syn}) generated using the surface temperature distribution on the Hayabusa capsule surface from [23]. This process tests the ability of the peak temperature model based on empirical relations (Equations (4) and (5)) to accurately identify peak temperatures from spectral signatures created using an independent temperature profile. The 51 km dataset (see Figure 4) was selected as representative of a high surface temperature condition where $T_{max} = 3330$ K. Results for two synthesised cases are presented:

- (a) an idealised theoretical case with no intervening atmosphere or noise (Section VII.A); and
- (b) signals containing random noise and atmospheric effects (Section VII.B).

For all cases the slant and tilt angle ranges (see Figure 5) were 0° to 90° respectively, which is a sweep of all view angles from a ‘front-on’ view to a ‘side-on’ view perpendicular to the velocity vector of the vehicle. For practical measurements, wake signal effects are minimised at small view angles and the back-shell of a sphere-cone is not visible

until the view angle exceeds the cone half angle. Therefore, although a high-temperature radiating shock layer is present, the region of greatest certainty in the present analysis is for view angles less than the cone half-angle. Analyses at larger view angles are presented to demonstrate the potential of the proposed peak temperature method, however further studies using well-defined spectral signatures inclusive of the entire radiating volume on and around the geometry are required, especially for large view angles.

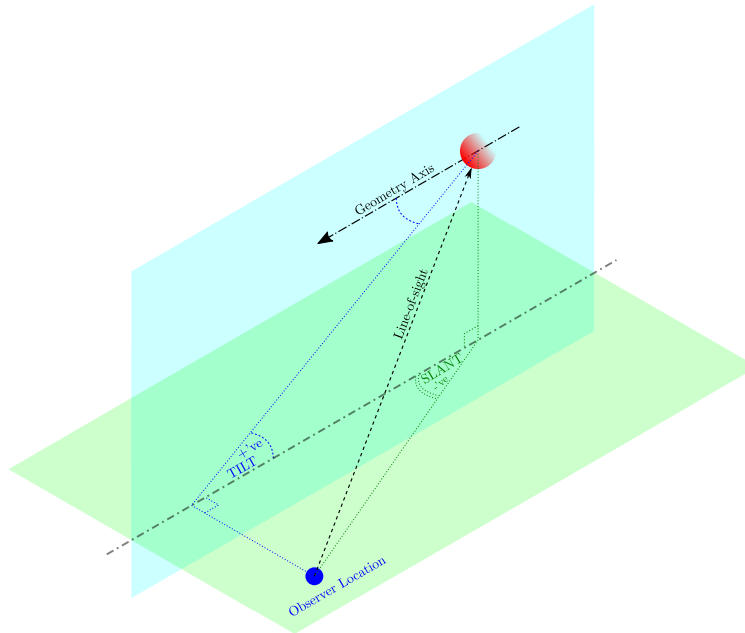


Fig. 5 Definition of tilt and slant angle.

To demonstrate the signal intensity curve fitting and resulting identification of the capsule surface temperature for the existing effective temperature model and for the new peak temperature model, a noise-free intensity signal (I_{syn}) was generated. This idealised noise free signal used a published surface temperature distribution for the Hayabusa capsule (the 51 km dataset from [23]) to define the surface temperature distribution– a process which is detailed in Section VII.A. Two curve fits were completed for every I_{syn} : (1) $I_{T_{\text{eff}}}$ an effective temperature curve fit using Equation (7) where $T(s)$ is a constant; and (2) $I_{T(s)}$, described herein as the peak temperature method, which uses Equation (7) where $T(s)$ is described by Equations (4) and (5). The objective of the curve fitting process is to minimise the quantities $\sum_{\text{all } \lambda} (I_{T_{\text{eff}}} - I_{\text{syn}})^2$ and $\sum_{\text{all } \lambda} (I_{T(s)} - I_{\text{syn}})^2$ for the effective temperature (T_{eff}) and peak temperature (T_{peak}) models respectively.

The normalised signal intensity for the front-on view (0° tilt and slant angles) is presented in Figure 6a, along with the error of the curve fitting for the effective temperature and peak temperature models. Relative to the effective temperature method, the error of the signal intensity fitting step is significantly reduced by new peak temperature identification method for each instrument tested. The identified surface temperatures from the cases in Figure 6a are presented in Figure 6b and compared to the surface temperature distribution used to generate the intensity signal. Figure 6b shows

that: (1) the empirical method is a suitable approximation for the surface temperature data from [23]; and (2) that the sensitivity of the effective temperature approach to the wavelengths which are resolved can be largely overcome using the peak temperature method. The wavelength dependence for each model is further explored in Section VII. The maximum surface temperature of the capsule was well resolved by the peak temperature model, with the resolution along the wetted length primarily limited by the empirical models (Equations (4) and (5)).

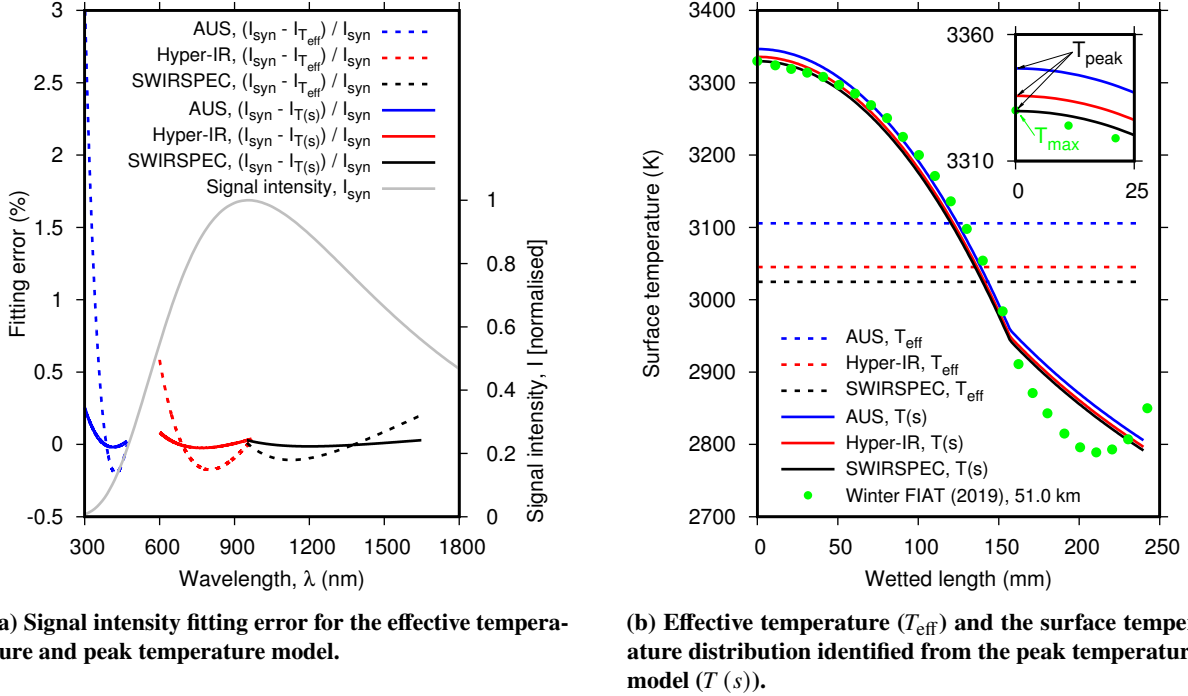


Fig. 6 Signal intensity and the identified capsule surface temperature for a front-on view of the Hayabusa capsule at 51.0 km altitude. The surface temperature distribution of the capsule was defined from the simulated 51.0 km altitude results in [23].

VII. Results

A. Case 1- Intensity Signals without Noise or an Intervening Atmosphere

The performance of the effective temperature and peak surface temperature models is first investigated in the ideal situation of a noise-free measured spectral irradiance signal with no intervening atmosphere. Such a case is physically unrealistic, however it forms a benchmark performance level which is built upon in Section VII.B. The radiance signal was generated for slant and tilt angles from 0° to 90° using the 51 km dataset from [23] where $T_{\text{max}} = 3330$ K, which is shown in Figure 6b. The ideal spectral intensity signals were processed for three virtual spectrometers using Equation (7) at the known view angles to determine the ideal response for the effective temperature and peak temperature models as presented in Figure 7.

As expected, for the three spectrometers assessed, the effective temperature model results in a temperature less than

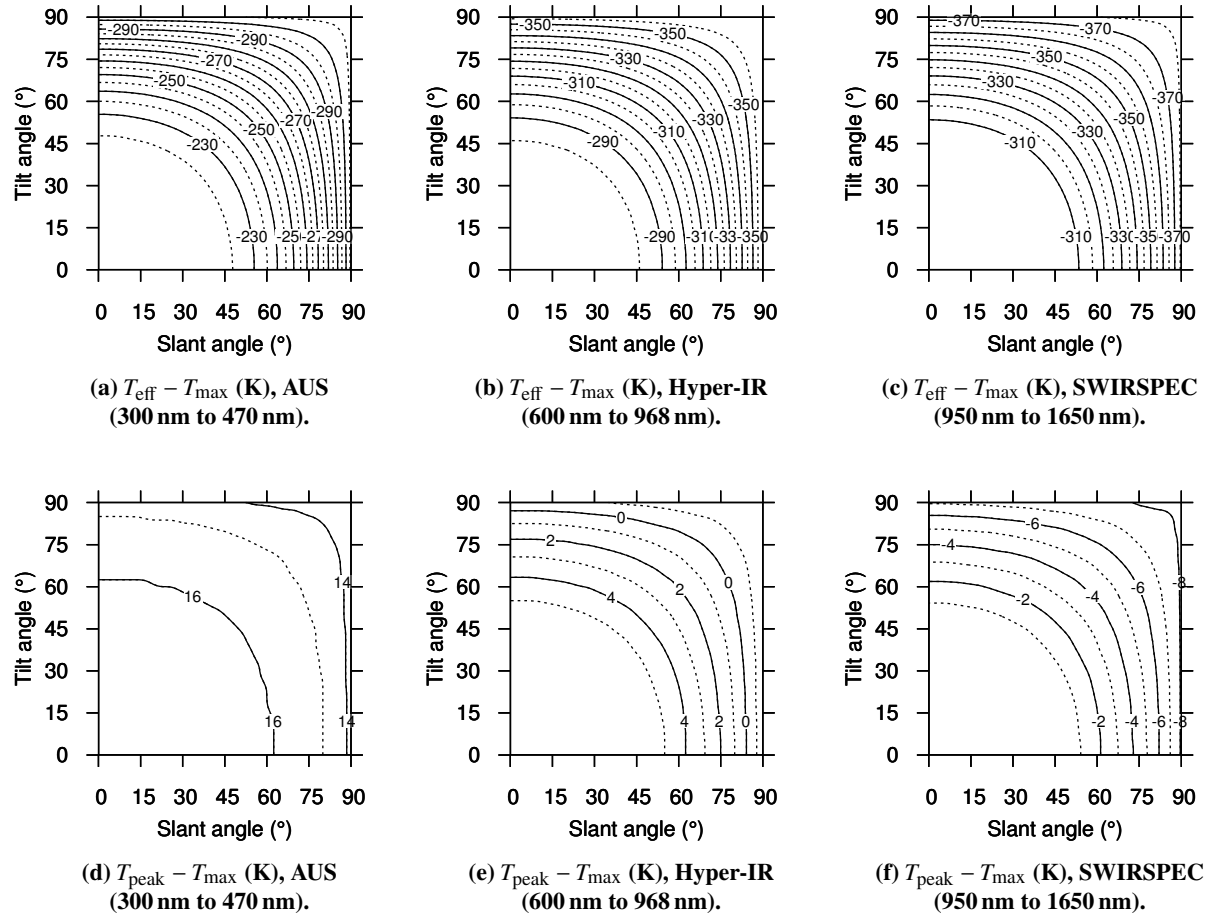


Fig. 7 Difference between the defined maximum surface temperature ($T_{\text{max}} = 3330$ K) of the Hayabusa sample return capsule and the identified temperature using the effective temperature (T_{eff}) and peak temperature (T_{peak}) models using ideal radiance measurements for three virtual spectrometers.

the defined maximum surface temperature as shown in Figures 7a to 7c. At front-on view angles, the AUS instrument had the smallest difference from the defined maximum temperature (-225 K), however agreement across the different instruments was within 85 K. For view angles less than 45° (the half-angle of the geometry), the effective temperature of the capsule is between 91% and 94% of the maximum temperature of the capsule. Such agreement suggests that it may be possible to produce a look-up table of corrections to apply to the effective temperature to better identify the peak capsule temperature, however this is shown in VII.B to be a flawed approach for realistic spectral signatures. The magnitude of the difference between the defined maximum temperature and effective temperature increases with increasing view angle.

The peak temperature model (results shown in Figures 7d to 7f) was able to resolve the defined maximum temperature of the capsule geometry (3330 K) to within a maximum error of 16 K which was for the AUS instrument at small view angles. Excellent agreement was found across all three instruments used, demonstrating that the new peak temperature

method may be a more suitable method than the established effective temperature method for reporting the surface temperatures of hot bodies measured using remote observations.

B. Case 2- Radiance Signals with Noise and Atmospheric Effects

To further investigate the performance of the effective and peak temperature identification models, synthetic spectral signatures with measurement noise and atmospheric effects were created. The spectral signatures were generated for the Hayabusa sample return capsule at 51 km, which is the same condition used in Section VII.A. Individual spectral signatures were generated for each of the three virtual spectrometers so that the signal-to-noise ratio could be independently set for each spectrometer.

Synthetic spectral intensity signals with noise ($I_{\text{syn,n}}$) were generated using

$$I_{\text{syn,n}}(\lambda) = \frac{I_{\text{syn}}(\lambda) \times \tau(\lambda) + I_{\text{noise}}}{\tau(\lambda)} \quad (8)$$

where I_{syn} is the ideal noise-free spectral intensity, I_{noise} is Gaussian white noise added to the signal, and $\tau(\lambda)$ is the atmospheric transmission. The intention of the noise addition is to introduce some representative noise at the simulated detector such that a representative noise-to-signal ratio is obtained. Considering the limiting case of complete extinction due to atmospheric absorption ($\tau = 0$), the noise-to-signal ratio will go to infinity which is demonstrating more uncertainty when the atmospheric transmission is low.

In the cases presented herein, $\tau(\lambda)$ was the 51 km capsule altitude model presented by [23]. The amplitude of I_{noise} is defined such that when $\tau(\lambda)$ is set to unity the root-mean-square (RMS) noise level is approximately 10%. Due to the lower intensity of the spectral radiance at ultraviolet wavelengths, the AUS instrument is likely to have a higher level of measurement noise than the Hyper-IR and SWIRSPEC instruments; however the noise level is a function of the instrumentation quality, instrumentation settings, optical path length, view angles, tracking quality, and other variables. Therefore, although higher or lower noise levels may be encountered in practice, 10% RMS noise for all instruments was selected for further analysis. Since the identified effective temperature and peak temperature changes with the noise signal, the analysis was repeated 200 times to produce maps of the mean identified temperature and standard deviation of this identified temperature, which are presented as Figure 8 (effective temperature) and Figure 9 (peak temperature).

In the presence of random noise and atmospheric effects, the effective temperature model produces significantly different results from the ideal case (Figure 7). Because of the noise and atmospheric effects, the minimum wavelength used for the AUS instrument was increased from 300 nm to 320 nm. The most pronounced changes in the results are for the Hyper-IR instrument where the effective temperature is approximately 350 K lower than for the noise-free case; and for the SWIRSPEC instrument where the effective temperature is approximately 430 K higher than for the noise-free case. Such significant changes to the effective temperature in the presence of noise demonstrate that simply producing

look-up tables of corrections to adjust the effective temperature is not a valid way to better understand the surface temperature on the capsule, nor for comparing experimental data obtained from different instruments.

For each of the three instruments tested, the effective temperature is insensitive to view angle when the view angle is less than 45° (the Hayabusa capsule half angle) as shown in Figures 8a to 8c. However, the effective temperature is a function of the wavelengths which are resolved by the instrument. The standard deviation of the datasets are shown in Figures 8d to 8f show the sensitivity of the effective temperature to signal noise. The standard deviation for the AUS instrument (Figure 8d) remains less than 20 K and exhibits no trends with varying view angle. For the Hyper-IR instrument, the highest standard deviations tend to occur at small view angles, with magnitudes up to 60 K, which is about 2% of the effective temperature (2740 K) at small view angles. For the SWIRSPEC instrument, the standard deviation was between 50 K and 100 K with no trends apparent.

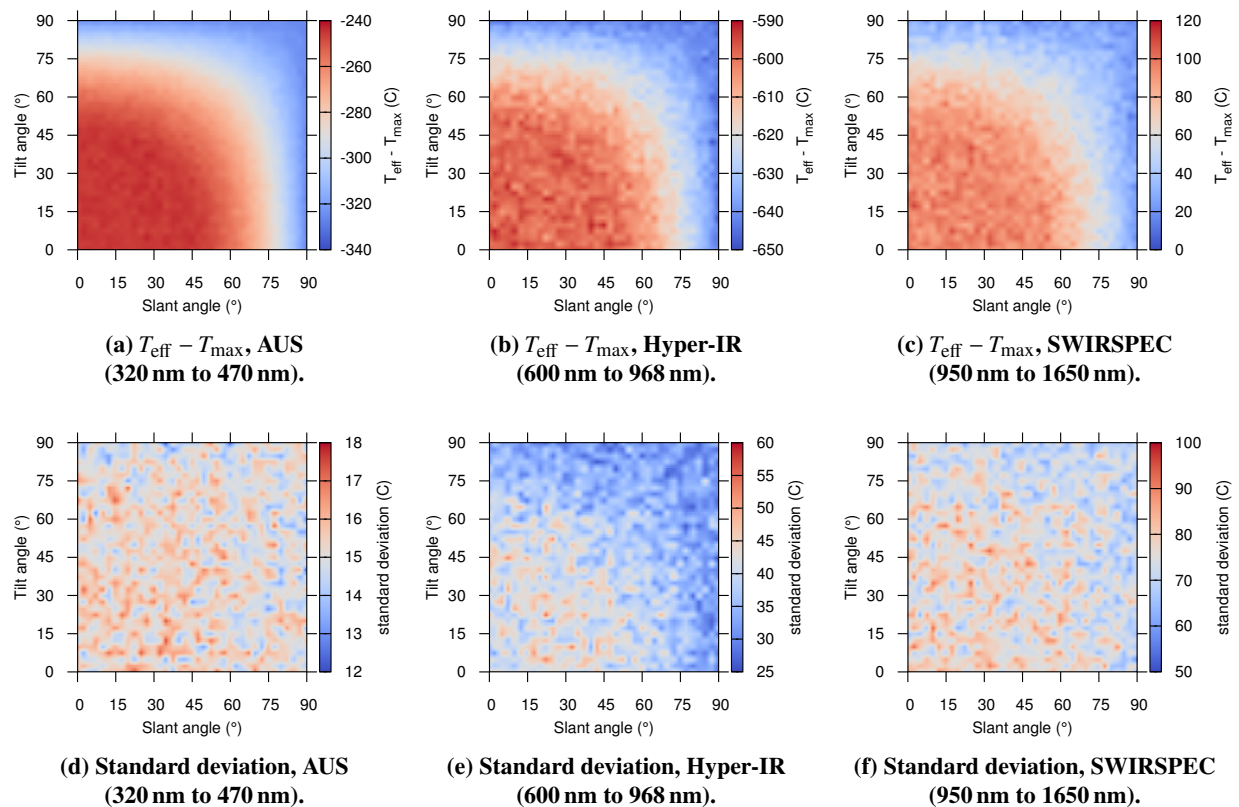


Fig. 8 Difference between the known maximum surface temperature ($T_{\text{max}} = 3330 \text{ K}$) and effective temperature for the Hayabusa capsule as measured from three virtual instruments using synthetic spectral signatures generated using the 50 km altitude surface temperature data from [23] with 10% RMS measurement noise.

The same spectral signatures analysed using the effective temperature method were analysed using the new peak temperature identification method to produce the maps shown in Figure 9. The maximum difference between the known maximum surface temperature and identified peak temperature is for the AUS instrument at 17 K which is an error of

0.5% relative to T_{\max} . This error further reduces for the Hyper-IR and SWIRSPEC instruments. For all instruments, the difference between the minimum and maximum peak temperature for view angles from 0° to 90° was an order of magnitude smaller than for the effective temperature method.

The identified peak temperature is consistent across all three instruments, which is a significant improvement over the established effective temperature method which cannot be used to compare the results from different instruments and view angles with any certainty. For all instruments, the standard deviation for the 200 peak temperature datasets was significantly lower than for the effective temperature method. The small standard deviations for the peak temperature method suggest that the method is robust.

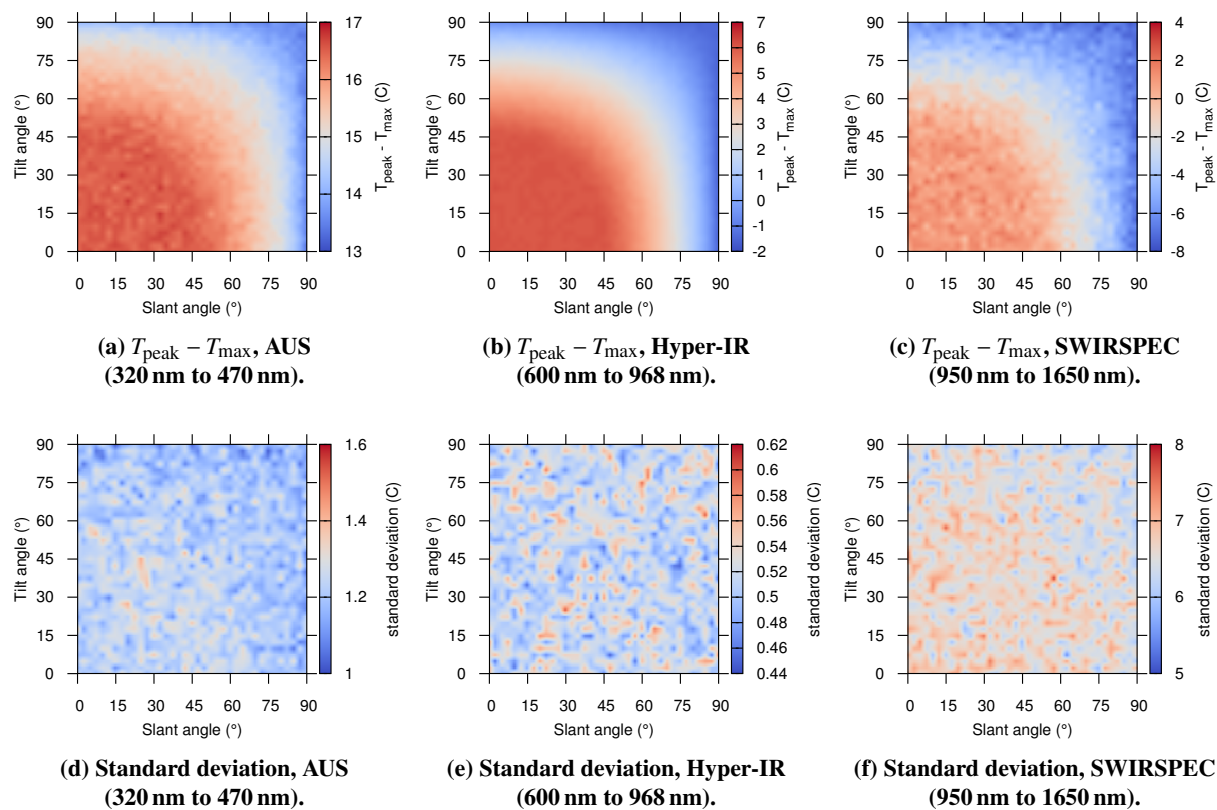


Fig. 9 Difference between the known maximum surface temperature ($T_{\max} = 3330$ K) and identified peak temperature (T_{peak}) for the Hayabusa capsule as measured from three virtual instruments using synthetic spectral signatures generated using the 50 km altitude surface temperature results from [23] with approximately 10% RMS measurement noise.

C. Current Limitations

The present investigation of the performance of the peak temperature method has shown that the method is robust and can be used to identify the peak temperature of a 45° degree half angle sphere-cone (the Hayabusa sample return capsule) using similar assumptions that are made for the established effective temperature method. An investigation of

the performance of the peak temperature model should be completed for other geometries that are of interest where temperature distributions can be defined from high-fidelity simulations.

The validity of the assumption that emissions from the shock layer, wake, and rear surface of the geometry can be neglected should be investigated using high-order models to generate synthetic spectral signatures through a range of view angles. Using high-order methods to create synthetic spectral signatures inclusive of gas effects is currently used to compare the results of numerical simulations to experimentally measured spectral irradiance from remote observations, so this is a clear development opportunity.

The time-invariant scaling of the surface temperature distribution is noted as a limitation of numerical studies [19]. As shown in Figure 4, the present empirical correlations are suitable for the Hayabusa geometry, however studies should be made to identify for what geometries the empirical models may require time dependence to be included.

VIII. Conclusions

Remote observations of real hypervelocity events are critical to the understanding of the associated aerothermal environment and the subsequent development of safe and efficient materials and geometries. However, the analysis of experimental data from these rare observations is currently limited. The common and established method for reporting surface temperature results from remote observations is the effective temperature method which was shown to be unsuitable for quantitative comparison from different instruments due to its sensitivity to the view angles, resolved wavelengths and measurement noise. A new method which identifies the peak surface temperature on a body was developed and investigated using a published surface temperature on the forebody of the Hayabusa sample return capsule. The next step in the method development and validation is to apply the method to spectra generated from high-fidelity CFD for complete and specific geometries and gas fields, which would then allow the confident application of the method to real measured data. This peak-temperature method can be used to directly compare the results obtained from different instruments and view angles, which overcomes a significant limitation of the effective temperature method. The ability of the peak temperature method to identify the maximum surface temperature on a body is valuable for numerical studies which require knowledge of often proprietary heat shield materials for the best results. Through experimental identification of the peak temperature on a geometry, simulation specialists have a key parameter for comparison with their assumed or known material.

Acknowledgments

This project was funded by the Australian Government through the Australian Research Council Linkage Project LP210301072. Fabian Zander is funded by the Australian Research Council through the Discovery Early Career Researcher Award number DE200101674. This research was undertaken using the University of Southern Queensland (UniSQ) Fawkes HPC which is co-sponsored by QCIF (Queensland Cyber Infrastructure Foundation)

References

- [1] Wright, W., and Wright, O., “First flight, 120 feet in 12 seconds, 10:35 a.m.; Kitty Hawk, North Carolina,” , 1903. URL <https://www.loc.gov/pictures/item/00652085/>.
- [2] Jenkins, D. R., and Landis, T. R., *Hypersonic: the story of the North American X-15*, Crecy, 2003.
- [3] “Report of the Presidential Commission on the Space Shuttle Challenger Accident,” Volumes I-V, June 1986.
- [4] “Columbia Accident Investigation Board Report,” Volume 1, NASA, August 2003.
- [5] Horvath, T., Tomek, D., Splinter, S., Zalameda, J., Krasa, P., Schwartz, R., Gibson, D., Tietjen, A., and Berger, K., “The Hythirm Project: Flight Thermography of the Space Shuttle During Hypersonic Re-Entry,” *48th AIAA Aerospace Sciences Meeting Including the New Horizons Forum and Aerospace Exposition*, AIAA, Orlando, FL, 2010. <https://doi.org/10.2514/6.2010-241>.
- [6] Schwartz, R. J., McCrear, A. C., Gruber, J. R., Hensley, D. W., Verstynen, H. A., Oram, T. D., Berger, K. T., Splinter, S. C., Horvath, T. J., and Kerns, R. V., “Remote infrared imaging of the space shuttle during Hypersonic flight: HYTHIRM mission operations and coordination,” *42nd AIAA Thermophysics Conference*, 2011. <https://doi.org/10.2514/6.2011-3326>.
- [7] Horvath, T. J., Cagle, M. F., Grinstead, J. H., and Gibson, D. M., “Remote observations of reentering spacecraft including the space shuttle orbiter,” *IEEE Aerospace Conference Proceedings*, 2013. <https://doi.org/10.1109/AERO.2013.6497380>.
- [8] Jenniskens, P., Wercinski, P., Olejniczak, J., Wright, M., Raiche, G., Kontinos, D., Desai, P., Spalding, R., Sandquist, K., Rossano, G., Russell, R., Revelle, D., Hladiuk, D., and Hildebrand, A., “Surface Heating from Remote Sensing of the Hypervelocity Entry of the NASA GENESIS Sample Return Capsule,” *44th Aerospace Sciences Meetings*, American Institute of Aeronautics and Astronautics, 2006. <https://doi.org/10.2514/6.2006-381>, URL <http://dx.doi.org/10.2514/6.2006-381>.
- [9] Löhle, S., Wernitz, R., Herdrich, G., Fertig, M., Röser, H. P., and Ritter, H., “Airborne re-entry observation experiment SLIT: UV spectroscopy during STARDUST and ATV1 re-entry,” *CEAS Space Journal*, Vol. 1, No. 1-4, 2011, pp. 59–69. <https://doi.org/10.1007/s12567-010-0005-3>.
- [10] Grinstead, J., Jenniskens, P., Cassell, A., Albers, J., and Winter, M., “Airborne Observation of the Hayabusa Sample Return Capsule Re-entry,” *Fluid Dynamics and Co-located Conferences*, American Institute of Aeronautics and Astronautics, 2011, pp. –. URL <http://dx.doi.org/10.2514/6.2011-3329>.
- [11] Buttsworth, D., Morgan, R., and Jenniskens, P., “Near-Ultraviolet Emission Spectroscopy of the Hayabusa Reentry,” *Journal of Spacecraft and Rockets*, Vol. 50, No. 6, 2013, pp. 1109–1120. URL <http://dx.doi.org/10.2514/1.A32500>.
- [12] Scott, C. F., and Inman, J. A., “SCIFLI Airborne Observation of the Hayabusa2 Sample Return Capsule Re-Entry,” American Institute of Aeronautics and Astronautics (AIAA), 2022. <https://doi.org/10.2514/6.2022-3798>.

- [13] Zander, F., Buttsworth, D. R., Birch, B., Noller, L., Wright, D., James, C. M., Thompson, M., Apirana, S., Leis, J., Lobsey, C., and Payne, A., “Australian Rapid-Response Airborne Observation of the Hayabusa2 Reentry,” *Journal of Spacecraft and Rockets*, Vol. 58, No. 6, 2021, pp. 1915–1919. <https://doi.org/10.2514/1.A35062>.
- [14] Birch, B., Zander, F., Buttsworth, D., Noller, L., and Payne, A., “Hayabusa2 Capsule Reentry: Visible and Near-IR Emission Spectroscopy from the Australian Airborne Observation,” *AIAA AVIATION 2022 Forum*, American Institute of Aeronautics and Astronautics, 2022. <https://doi.org/10.2514/6.2022-3736>, URL <https://arc.aiaa.org/doi/10.2514/6.2022-3736>.
- [15] Jenniskens, P., Albers, J., Koop, M., Odeh, M., Al-Noimy, K., Al-Remeithi, K., Al-Hasmi, K., Dantowitz, R., Gasdia, F., Loehle, S., Zander, F., Hermann, T., Farnocchia, D., Chesley, S., Chodas, P., Park, R., Giorgini, J., Gray, W., Robertson, D., and Lips, T., “Airborne Observation of an Asteroid Entry for High Fidelity Modeling: Space Debris Object WT1190F,” *AIAA Science and Technology Forum and Exposition*, AIAA, San Diego, CA, 2016.
- [16] Vaubaillon, J., Loir, C., Ciocan, C., Kandeepan, M., Millet, M., Cassagne, A., and Lacassagne, L., “A 2022 τ -Herculid meteor cluster from an airborne experiment : automated detection , characterization , and consequences for meteoroids,” *Astronomy & Astrophysics*, , No. 2017, 2023, pp. 1–6. <https://doi.org/10.1051/0004-6361/202244993>.
- [17] Loehle, S., Zander, F., Lemmens, S., and Krag, H., “Airborne Observations of Re-entry Break-up: Results and Prospects,” *7th European Conference on Space Debris*, 2017, p. 5 pp.
- [18] Jenniskens, P., Albers, J., Koop, M. W., Odeh, M. S., Al-Noimy, K., Al-Remeithi, K., Al Hasmi, K., Dantowitz, R. F., Gasdia, F., Löhle, S., Zander, F., Hermann, T., Farnocchia, D., Chesley, S. R., Chodas, P. W., Park, R. S., Giorgini, J. D., Gray, W. J., Robertson, D. K., and Lips, T., “Airborne observations of an asteroid entry for high fidelity modeling: Space debris object WT1190F,” *54th AIAA Aerospace Sciences Meeting*, , No. SciTech, 2016, pp. 4–8.
- [19] Prabhu, D. K., Saunders, D. A., Cruden, B. A., and Grinstead, J. H., “Simulations of Hayabusa2 Atmospheric Entry and Comparisons with Data from the Imaging Campaign,” *AIAA AVIATION 2022 Forum*, 2022, pp. 1–24. <https://doi.org/10.2514/6.2022-3800>.
- [20] Kraetzig, B., Löhle, S., and Buttsworth, D. R., “Evolution of Plasma Species and Heat-Shield Temperatures from Hayabusa Reentry Observation,” *Journal of Spacecraft and Rockets*, Vol. 51, No. 3, 2014, pp. 823–837. <https://doi.org/10.2514/1.A32854>.
- [21] Winter, M., and Herdrich, G., “Spectroscopic Observation of the STARDUST Re-Entry in the Near UV,” *39th AIAA Thermophysics Conference*, American Institute of Aeronautics and Astronautics, Reston, Virginia, 2007, pp. 1–12. <https://doi.org/10.2514/6.2007-4050>, URL <https://arc.aiaa.org/doi/10.2514/6.2007-4050>.
- [22] Loehle, S., Eberhart, M., Zander, F., Meindl, A., Rudawska, R., Koschny, D., Zender, J., Dantowitz, R., and Jenniskens, P., “Extension of the plasma radiation database PARADE for the analysis of meteor spectra,” *Meteoritics and Planetary Science*, Vol. 56, No. 2, 2021, pp. 352–361. <https://doi.org/10.1111/maps.13622>.

- [23] Winter, M. W., McDaniel, R. D., Chen, Y.-K., Saunders, D., and Jenniskens, P., “Radiation Modeling for Reentry of Hayabusa Sample Return Capsule,” *Journal of Spacecraft and Rockets*, Vol. 56, No. 4, 2019, pp. 1152–1164. <https://doi.org/10.2514/1.A34381>.
- [24] Tanno, H., Yamada, T., Dantowitz, R., Hoover, Z., Lockwood, C., Klemm, C., Scott, C., Conn, R., Nowicki, M., Inmann, J., Scriven, G., Brown, C., and Grinstead, J., “Analysis of Surface Temperature of Hayabusa 1 & 2 SRC in Airborne Spectroscopy Measurement,” *AIAA AVIATION 2022 Forum*, 2022, pp. 1–13. <https://doi.org/10.2514/6.2022-3733>.
- [25] Löhle, S., Mezger, A., and Fulge, H., “Measured surface temperatures of the Hayabusa capsule during re-entry determined from ground observation,” *Acta Astronautica*, Vol. 84, 2013, pp. 134–140. <https://doi.org/https://doi.org/10.1016/j.actaastro.2012.11.004>, URL <https://www.sciencedirect.com/science/article/pii/S0094576512004511>.
- [26] Buttsworth, D., and Buttsworth, T., “Deducing flux from single point temperature history when relative spatial variation of flux is prescribed,” *International Journal of Heat and Mass Transfer*, Vol. 181, 2021, p. 121831. <https://doi.org/https://doi.org/10.1016/j.ijheatmasstransfer.2021.121831>, URL <https://www.sciencedirect.com/science/article/pii/S0017931021009364>.
- [27] Kemp, N., Rose, R., and Detra, R., “Laminar heat transfer around blunt bodies in dissociated air,” *J. Aero Space Sci*, Vol. 26, No. 7, 1959, p. 421.
- [28] Fahy, E. J., Buttsworth, D. R., Gollan, R. J., Jacobs, P. A., Morgan, R. G., and James, C. M., “Experimental and computational fluid dynamics study of hayabusa reentry peak heating,” *Journal of Spacecraft and Rockets*, Vol. 58, No. 6, 2021, pp. 1833–1846. <https://doi.org/10.2514/1.A34863>.